Original Article

Predicting the Ki-67 proliferation index in cervical cancer: a preliminary comparative study of four non-Gaussian diffusion-weighted imaging models combined with histogram analysis

Yun Su[1#], Kunjie Zeng[1#], Zhuoheng Yan[1], Xiaojun Yang[1], Lingjie Yang[1,2], Lu Yang[1], Riyu Han[1], Fengqiong Huang[1], Hong Deng[1*], Xiaohui Duan[1,2*]

[1]Department of Radiology, Sun Yat-sen Memorial Hospital, Sun Yat-sen University, Guangzhou, China; [2]Guangdong Provincial Key Laboratory of Malignant Tumor Epigenetics and Gene Regulation, Medical Research Center, Sun Yat-sen Memorial Hospital, Sun Yat-sen University, Guangzhou, China

Contributions: (I) Conception and design: X Duan, H Deng; (II) Administrative support: Y Su, K Zeng; (III) Provision of study materials or patients: Z Yan, X Yang, Lingjie Yang; (IV) Collection and assembly of data: K Zeng, Lu Yang, R Han; (V) Data analysis and interpretation: H Deng, Y Su, F Huang; (VI) Manuscript writing: All authors; (VII) Final approval of manuscript: All authors.

[#]These authors contributed equally to this work.

[*]These authors contributed equally to this work as corresponding authors.

Correspondence to: Hong Deng, MB. Department of Radiology, Sun Yat-sen Memorial Hospital, Sun Yat-sen University, 107 Yanjiang West Road, Guangzhou 510120, China. Email: dengh53@mail.sysu.edu.cn; Xiaohui Duan, MD. Department of Radiology, Sun Yat-sen Memorial Hospital, Sun Yat-sen University, 107 Yanjiang West Road, Guangzhou 510120, China; Guangdong Provincial Key Laboratory of Malignant Tumor Epigenetics and Gene Regulation, Medical Research Center, Sun Yat-sen Memorial Hospital, Sun Yat-sen University, 107 Yanjiang West Road, Guangzhou 510120, China. Email: duanxh5@mail.sysu.edu.cn.

Background: The prognosis for patients with cervical cancer (CC) is strongly correlated with the Ki-67 proliferation index (PI). However, the Ki-67 PI obtained through biopsy has certain limitations. The non-Gaussian distribution diffusion model of magnetic resonance imaging (MRI) may play an important role in characterizing tissue heterogeneity. At present, there are limited data available concerning the prediction of Ki-67 PI using models based on histogram features of non-Gaussian diffusion distribution. This study aimed to determine whether preoperative histogram features from multiple non-Gaussian models of diffusion-weighted imaging can predict the Ki-67 PI in patients with CC.

Methods: Our cross-sectional prospective study recruited a total of 53 patients suspected of having CC who underwent 3.0-T MRI at Sun Yat-sen Memorial Hospital of Sun Yat-sen University between January 2022 and January 2023. Fifteen b values (0–4,000 s/mm^2) were used for diffusion-weighted imaging. A total of nine parameters from four non-Gaussian diffusion-weighted imaging models, including continuous-time random walk (CTRW), diffusion kurtosis imaging (DKI), fractional order calculus (FROC), and intravoxel incoherent motion (IVIM), were used. Whole-tumor volumetric histogram analysis of these parameters was then obtained. In logistic regression, significant histogram characteristics were statistically examined across two groups to build the final prediction model. To assess diagnostic parameters of the proposed model in the diagnosis of the Ki-67 PI, along with the sensitivity, specificity, and diagnostic accuracy of these various parameters from the four models, receiver operating feature analysis was applied.

Results: Among the 53 patients (55.3±9.6 years, ranging from 23 to 79 years) included in the study, 15 had a Ki-67 PI ≤50% and 38 had a Ki-67 PI >50%. Univariable analysis determined that 12 histogram features were statistically different between the two groups. In multivariable logistic regression, we ultimately selected 6 histogram features to construct the final prediction model, with CTRW_α_10th percentile [odds ratio (OR)

=0.955; 95% confidence interval (CI): 0.92–0.99; P=0.019], CTRW_α_robust mean absolute deviation (OR =0.893; 95% CI: 0.81–0.99; P=0.028), and CTRW_α_uniformity (OR =0.000, 95% CI: 0.00–0.90, P=0.047) being the independent predictive variables. The area under the curve of the combined prediction model was 0.845 (95% CI: 0.74–0.95), with a sensitivity of 78.9% (95% CI: 0.63–0.90), a specificity of 86.7% (95% CI: 0.60–0.98), an accuracy of 81.1% (95% CI: 0.68–0.91), a positive predictive value of 93.8% (95% CI: 0.79–0.99), and a negative predictive value of 61.9% (95% CI: 0.38–0.82).

Conclusions: The histogram features of multiple non-Gaussian diffusion-weighted imaging can help to predict the Ki-67 PI of CC, providing a new method for the noninvasive evaluation of critical biological features of CC.

Keywords: Ki-67 proliferation index (Ki-67 PI); cervical cancer (CC); continuous-time random-walk; histogram analysis; non-Gaussian diffusion-weighted imaging

Submitted Mar 21, 2024. Accepted for publication Aug 20, 2024. Published online Sep 26, 2024.
doi: 10.21037/qims-24-576
View this article at: https://dx.doi.org/10.21037/qims-24-576

Introduction

Cervical cancer (CC) is a prevalent form of malignant tumor in females globally, ranking highest in frequency after breast cancer, colorectal cancer, and lung cancer (1). Surgery combined with radiotherapy and chemotherapy is the primary treatment for patients with CC (2). However, a significant portion of patients with CC have unsatisfactory long-term survival. Previous studies have revealed that tumor proliferation is crucial in informing diagnoses, selecting treatment, and predicting prognosis in CC (3,4). Ki-67, as a protein in the nucleus of growing cells, is a reliable predictor of tumor proliferation. Studies have demonstrated a connection between the expression of the Ki-67 proliferation index (PI) and poor prognosis in breast cancer, non-small cell adenocarcinoma, and CC (4-6). At present, biopsy with immunohistochemical staining remains the prevalent method for preoperatively assessing the Ki-67 PI. However, biopsy is invasive and commonly fails to comprehensively characterize intratumoral heterogeneity due to the limited sample size of the biopsy. Therefore, using noninvasive imaging techniques to preoperatively determine the Ki-67 PI of the entire tumor is critical.

Magnetic resonance imaging (MRI) provides high-resolution images of soft tissues, enabling precise assessment of cervical lesions and their relationship with the muscular layer. It is widely used for diagnosis, staging, and evaluate of treatment efficacy in CC. However, although conventional MRI can primarily assess the morphological features of lesions, it has limited utility in determining the Ki-67 PI of CC and is thus challenged in effectively evaluating the prognosis of CC. Diffusion-weighted imaging (DWI) is extensively employed to predict invasiveness, evaluate treatment efficacy, and distinguish between benign and malignant cervical tumors via the examination the diffusion patterns of water molecules within tumorous tissue. DWI and its derived advanced diffusion sequences have been widely used to assess the Ki-67 PI in various tumors, especially in head and neck squamous cancer (7), endometrial carcinoma (8), and breast cancers (9). Only one previous study reported there to be an association between intravoxel incoherent motion (IVIM) and the Ki-67 PI in CC (10). IVIM, as a non-Gaussian distributed diffusion model, can characterize the diffusion of water molecules and the perfusion of microvessels simultaneously. Although a correlation between the degree of Ki-67 PI and pseudodiffusion coefficient (D*) has been established, this method cannot directly represent tissue heterogeneity in reflecting the Ki-67 PI in CC. In more recent years, numerous non-Gaussian diffusion models have been developed that are capable of evaluating data from a single scan through use of high b value and multi-b value diffusion sequences. These models include diffusion kurtosis imaging (DKI), IVIM, and the continuous-time random walk (CTRW) or their associated fractional-order calculus (FROC) model. These non-Gaussian diffusion models provide not only relevant parameters to describe water diffusion but also information regarding the temporal [the time required for water molecules to move (α)] and spatial [the distance that water molecules can diffuse (β)] heterogeneity of tissue microstructure (11). The histogram parameters of CTRW-DWI have been reported to play an

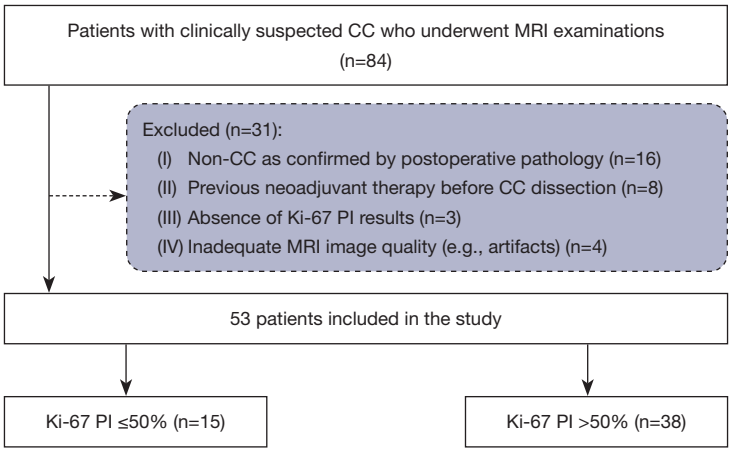

Figure 1 Workflow for enrollment of patients with CC according to Ki-67 PI value. CC, cervical cancer; MRI, magnetic resonance imaging; PI, proliferation index.

essential role in predicting the Ki-67 expression level in the breast tumor (12-14). However, the predictive performance of histogram features derived from these multiple non-Gaussian diffusion models for assessing the Ki-67 PI in CC remains unclear. Additionally, there is a lack of comparative experiments assessing the effectiveness of these four non-Gaussian diffusion models and their combined predictive ability in assessing the Ki-67 PI in CC.

The objective of this study was thus to evaluate the performance of histogram features derived from four non-Gaussian diffusion models and their combination in preoperatively predicting the Ki-67 PI in CC. The resulting findings may serve as evidence for informing clinical treatment decisions and prognosis evaluation in patients with CC. We present this article in accordance with the STROBE reporting checklist (available at https://qims.amegroups.com/article/view/10.21037/qims-24-576/rc).

Methods

Patients

The Institutional Ethics Committee of Sun Yat-sen Memorial Hospital of Sun Yat-sen University authorized and approved this prospective study (No. SYSEC-KY-KS-2022-057), and each patient completed an informed consent form. This study was conducted in accordance with the Declaration of Helsinki (as revised in 2013). We continuously recruited patients with suspected CC who underwent MRI at Sun Yat-sen Memorial Hospital of Sun Yat-sen University between January 2022 and January 2023. We used PASS version 21.0.3 software (NCSS LLC, Kaysville, UT, USA) for the estimation of sample size (N) before the study. A previous study reported that the texture analysis of the IVIM diffusion model yielded an area under the curve (AUC) of 0.816 in distinguishing a low and high Ki-67 PI in CC (10). We thus used this AUC to calculate the sample size, setting the values of α and power (1–β) as 0.05 and 0.9, respectively. Finally, we decided to include at least 15 patients in each group. The inclusion criteria were as follows: (I) pathologically confirmed CC, (II) multiple high b value diffusion sequences collected within 2 weeks before surgery or biopsy, and (III) missing Ki-67 PI results. Meanwhile, the exclusion criteria were as follows: (I) poor DWI images (serious motion and susceptibility artifacts), (II) missing Ki-67 PI values after surgery, (III) treatment before MRI examination, and (IV) a lesion size <5 mm on MR images. The participant flowchart is depicted in *Figure 1*.

MRI acquisition

MRI was performed using a 3.0-T scanner (MAGNETOM Vida; Siemens Healthineers, Erlangen, Germany) and a body phased-array coil with sensitivity encoding (SENSE) for receiving. Prior to contrast injection, axial DWI was performed using a single spin echo planar imaging session. The parameters of conventional pelvic scan and DWI sequence were as follows: axial gradient echo T1-weighted (T1W) Dixon sequence (repetition time/echo time: 5.3 ms/2.46 and 3.69 ms; field of view: 285 mm × 380 mm; matrix: 202×320; slice thickness: 1.2 mm; gap: 0.24 mm),

and axial fast spin-echo T2-weighted imaging (T2WI) sequence (repetition time/echo time: 2,650 ms/103 ms; field of view: 200 mm × 200 mm; matrix: 298×352; slice thickness: 3.5 mm; gap: 0.7 mm), an axial single-shot spin echo planar imaging DWI sequence [repetition time/echo time: 2,500 ms /84 ms; field of view: 248 mm × 248 mm; matrix: 124×124; slice thickness: 4 mm; interslice gap: 0.8 mm; SMS =2; b values: 0_1, 10_1, 20_1, 50_1, 80_1, 100_1, 150_1, 200_1, 400_1, 500_2, 800_2, $1{,}200_3$, $2{,}000_4$, $3{,}000_4$, and $4{,}000_5$ s/mm^2 (the subscript denotes the number of averages); gradient directions: x, y, and z; acquisition time: 3 min 56 s]. The apparent diffusion coefficient (ADC) value of conventional DWI was obtained with b values of 0 and 800 s/mm^2. All parametric maps were generated using a medical systems workstation from Siemens Healthineers.

Image analysis

Traditional DWI, which quantitatively measures ADC values, was automatically generated at medical system workstations and fitted using the following Eq. [1] (15):

$$S_b = S_0 \times e^{(-b \times ADC)} \quad [1]$$

where S_0 and S_b are the signal strengths at b values of 0 and 800, respectively. In addition, four no-Gaussian MRI diffusion models were fitted using MRStation software (Chengdu Zhongying Medical Technology Co., Ltd., Chengdu, China), which is based on DIPY (https://dipy.org/). For the DKI model, the highest b value of 3,000 was selected for fitting, and two diffusion metrics, Includes mean kurtosis value in DKI (DKI_K) and mean diffuse value in DKI (DKI_D), were calculated using the following Eq. [2] (16):

$$\frac{S_b}{S_0} = e^{\left(-b \times D_{app} + \frac{1}{6b^2} + D_{app}^2 \times K_{app}\right)} \quad [2]$$

where K_{app} is kurtosis, and D_{app} is the ADC based on non-Gaussian diffusion. The CTRW model, on the other hand, involved three diffusion metrics (CTRW_α, CTRW_β, and CTRW_D), which were calculated as Eq. [3] (17):

$$\frac{S_b}{S_0} = E_\alpha\left[-(b \times D)^\beta\right] \quad [3]$$

where Eα is the Mittag-Leffler function of α order; D is an anomalous diffusion coefficient; and parameters α and β are the diffusion metrics associated with temporal and spatial diffusion heterogeneities, respectively, and vary between 0 and 1, indicating homogeneity within the medium. Unlike CTRW, which employs a simple formula for calculation, FROC uses a relatively complex calculation method to derive three metrics (FROC_D, FROC_β, and FROC_μ), as follows Eq. [4] (18):

$$\frac{S_b}{S_0} = e^{\left[-D\mu^{2(\beta-1)} \times \left(\gamma^G \times d^\delta\right)^{2\beta} \times \left(\Delta - \frac{2\beta-1}{2\beta+1} \times \delta\right)\right]} \quad [4]$$

In this model, β and D describe the heterogeneity of spatial diffusion, while μ is a parameter that describes spatial diffusion. In the formula, Gd is the amplitude of the diffusion gradient, δ is the width of the gradient pulse, and Δ is the gradient lobe separation. Finally, the double exponential model was used to obtain the semidiffusion coefficient (D*) of IVIM Eq. [5] (15):

$$\frac{S_b}{S_0} = \left[(1-f)e^{(-b \times D)}\right] + \left[fe^{\left(-b \times D^*\right)}\right] \quad [5]$$

Tumor segmentation and histogram analysis

Two radiologists with 6 and 10 years of experience in pelvic disease diagnosis who were blinded to the clinical information and pathological results independently performed the primary tumor segmentation by manually delineating the volume of interest (VOI) of the whole tumor using ITK-SNAP version 3.6.0 software (www.itksnap.org) and conducted feature extraction for each patient. The average number of pixels for each VOI was also calculated. Through use of T2W and contrast-enhanced T1W imaging, areas of peritumoral edema and apparent necrotic components inside the tumor were ruled out. *Figure 2* shows the segmentation techniques that were employed.

Parametric map histogram analysis was carried out with the FeAture Explorer version 0.3.6 software (https://github.com/salan668/FAE). After extraction, 18 histogram features, including mean, median, maximum, mean absolute deviation, minimum, range, robust mean absolute deviation, root mean squared, skewness, total energy, variance, percentiles (10^{th} and 90^{th}), interquartile range, energy, kurtosis, uniformity, and entropy were obtained.

Pathological examination

One skilled pathologist with over 8 years of expertise in pathological diagnosis carried out the postoperative Ki-67 testing. Streptavidin peroxidase staining was carried

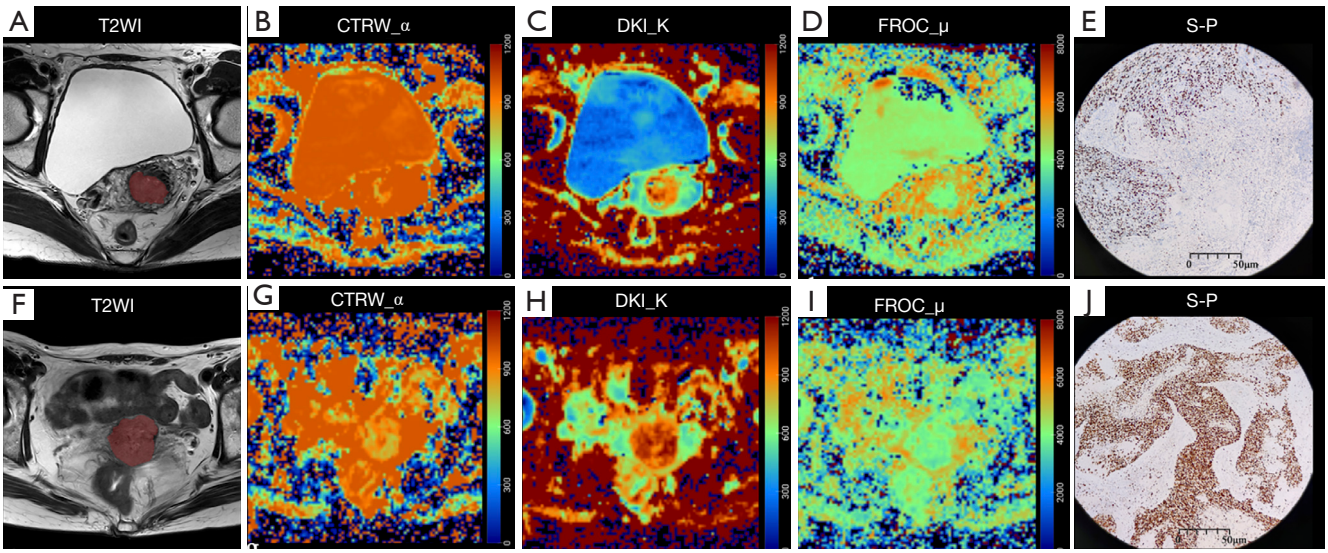

Figure 2 The T2WI, parametric maps, and pathological sections of two patients with cervical cancer. (A-E) Images from a 53-year-old female with cervical squamous cell carcinoma and a Ki-67 proliferation index ≤50%. (F-J) Images from a 65-year-old female with squamous cell carcinoma and a Ki-67 PI >50%. (A,F) Conventional T2-weighted images; the red area in the T2 weighted image represents the lesions contained in the volume of interest. (B-D,G-I) The pseudo-colorized images showing the (B,G) CTRW_α, (C,H) DKI_K, and (D,I) FROC_μ maps. (E,J) S-P-stained sections of cervical cancer (10×). T2WI, T2-weighted imaging; CTRW_α, α value of continuous-time random walk; DKI_K, MK value of diffusion kurtosis imaging; FROC_μ, μ value of fractional order calculus; S-P, streptavidin peroxidase; PI, proliferation index.

out in immunohistochemical staining. When distinct, brownish-yellow granules were observed in the cytoplasm of tumor cells and the staining intensity exceeded that of the nonspecific staining background, Ki-67 expression was considered positive. Ten fields with a 10× field of view were randomly selected, and the average tumor-positive percentage in each field was used as the Ki-67 PI. Two groups of patients were created: one with Ki-67 PI ≤50% and the other with Ki-67 PI >50%.

Statistical analysis

The data were analyzed with SPSS 22 software (IBM Corporation, Armonk, NY, USA). The interobserver agreement in the measurement of histogram features was assessed using the intraclass correlation coefficient (ICC), with an ICC >0.75 indicating good reliability. Normally distributed data are provided as the mean ± standard deviation (SD), and the difference in means between two groups was compared using the independent samples *t*-test. Nonnormally distributed data are provided as the median, and the difference in medians was determined via the Mann-Whitney test. A two-tailed P value <0.05 was deemed statistically significant. Statistically significant histogram features between the two groups were selected through multivariable logistic regression. We developed single parameter-based models and multiple parameter-based models to predict the Ki-67 expression level. To assess the models' sensitivity, specificity, and accuracy, the AUC and receiver operating characteristic (ROC) metrics were used. The DeLong test was used to compare the AUCs of various measures. The comparison of sensitivities, specificities, and accuracies between different metrics were compared with the McNemar test.

Results

Patients

This study recruited 86 participants. Among them, 8 cases received preoperative treatment, 3 cases had unclear pathological results, and 4 cases were excluded due to motion artifacts. Ultimately, 53 patients were included in this study. Of the 53 patients (55.3±9.6 years, ranging from 23 to 79 years), 15 had a Ki-67 PI ≤50% and 38 had a Ki-67 PI >50%. A histopathological evaluation was conducted on 53 patients with CC, of whom 39 were diagnosed with cervical squamous cell carcinoma (39/53, 73.58%) 12 with

Table 1 Clinicopathologic characteristics of the groups with Ki-67 PI ≤50% and Ki-67 PI >50%

Characteristic	Ki-67 PI ≤50% (n=15)	Ki-67 PI >50% (n=38)	P value
Age (years)	52.4±10.7	56.5±9.0	0.217*
Depth of invasion (mm)	1.8±1.0	2.0±1.3	0.656*
Pathological type (%)			0.978†
Cervical squamous cell carcinoma	10 (66.7)	29 (76.3)	
Cervical adenocarcinoma	5 (33.3)	7 (18.4)	
Invasive cancer	–	2 (5.3)	
Differentiation grade (%)			0.591†
Well differentiated	2 (13.3)	4 (10.5)	
Moderately differentiated	10 (66.7)	24 (63.2)	
Poorly differentiated	3 (20.0)	10 (26.3)	
Tumor FIGO staging (%)			0.534†
Stage T1	11 (73.3)	21 (55.3)	
Stage T2	1 (6.7)	8 (21.1)	
Stage T3	3 (20.0)	8 (21.1)	
Stage T4	–	1 (2.6)	
MRI-determined diameter of CC (cm)	3.4±1.2	3.9±1.7	0.337*

Data are presented as mean ± standard deviation or number (%). *, continuous variables were compared with the nonparametric test; †, categorical variables were compared with the Fisher exact test. PI, proliferation index; FIGO, International Federation of Gynecology and Obstetrics; MRI, magnetic resonance imaging; CC, cervical cancer.

cervical adenocarcinoma (12/53, 22.64%), and 2 with invasive cancer (2/53, 3.77%). Furthermore, there was no discernible difference between the two groups in terms of age, tumor histological stage, or tumor diameter (*Table 1*).

Univariable analysis

In reproducibility analysis, all histogram features exhibited excellent interobserver agreement (ICC ≥0.9). The average pixel count of VOI was 2,474.1±2,658.3. A total of 162 histogram features based on the multiple models of the DWI sequence were obtained. There were 12 histogram features with a statistical difference between the two groups (*Table 2*). Among them, 8 histogram features were from parameters of the CTRW model α, including 10^{th} percentile, entropy, mean, mean absolute deviation, robust mean absolute deviation, root mean squared, uniformity, and variance. In addition, histogram features with statistically significant differences between the two groups also included the minimum of parameter D and K from the DKI model and the minimum and 10^{th} percentile of parameter μ from the FROC model. Among them, CTRW_α_entropy (P=0.033), CTRW_α_mean absolute deviation (P=0.022), CTRW_α_robust mean absolute deviation (P=0.048), and CTRW_α_variance (P=0.028) values increases were associated with an increase in Ki-67 PI. The values of other histogram features were negatively correlated with the Ki-67 PI. In addition, there was no statistically significant difference in ADC values from conventional DWI sequences between the two groups.

Multivariable logistic regression

We performed univariable logistic regression on all variables, identifying 12 with statistical differences. Subsequently, we conducted multiple logistic regression on these 12 variables, and the final prediction model included 6 variables: CTRW_α_10^{th} percentile, CTRW_α_robust mean absolute deviation, CTRW_α_uniformity, CTRW_α_mean, DKI_K_minimum, and FROC_μ_10^{th} percentile. Among the P values of these variables, those of CTRW_α_10^{th} percentile [odds ratio (OR) =0.955; 95% confidence interval (CI): 0.92–0.99;

Table 2 Comparison of diffusion MRI quantitative metrics between the Ki-67 PI ≤50% and Ki-67 PI >50% groups

Parameter	Ki-67 PI ≤50% (n=15)	Ki-67 PI >50% (n=38)	P value
CTRW_α_10th percentile	776.4±138.8	670.0±141.2	0.031
CTRW_α_entropy	2.8±1.2	3.6 ±0.8	0.033
CTRW_α_mean	904.7±76.1	856.5±74.7	0.035
CTRW_α_mean absolute deviation	77.7±43.7	109.1±43.7	0.022
CTRW_α_robust mean absolute deviation	55.3±42.1	80.5±37.9	0.048
CTRW_α_root mean squared	912.0±70.6	869.7±65.9	0.044
CTRW_α_uniformity	0.3±0.2	0.2±0.1	0.035
CTRW_α_variance	$12.5\times10^3\pm10.9\times10^3$	$21.6\times10^3\pm16.6\times10^3$	0.028
DKI_D_minimum	725.0±445.9	429.9±390.7	0.013
DKI_K_minimum	141.5±179.1	27.5±98.7	0.006
FROC_μ_10th percentile	$3.5\times10^3\pm0.4\times10^3$	$2.7\times10^3\pm1.2\times10^3$	0.023
FROC_μ_minimum	644.0±1,108.2	187.1±676.4	0.014
ADC_value	760.4±105.2	755.5±104.9	0.880

Parameter data obtained from CTRW, FROC, DKI, and ADC of the Ki-67 PI ≤50% and Ki-67 PI >50% are presented as the mean ± standard deviation. P<0.05 indicates statistical significance. The table only displays histogram features with P values <0.05. MRI, magnetic resonance imaging; PI, proliferation index; CTRW_α, α value of continuous-time random walk; DKI_D, mean diffuse value of diffusion kurtosis imaging; DKI_K, mean kurtosis value of diffusion kurtosis imaging; FROC_μ, μ value of fractional order calculus; ADC, apparent diffusion coefficient.

P=0.019], CTRW_α_robust mean absolute deviation (OR =0.893, 95% CI: 0.81–0.99; P=0.028), and CTRW_α_uniformity (OR =0.000; 95% CI: 0.00–0.90; P=0.047) were less than 0.05, indicating these factors were independent predictors. The combined prediction model yielded an AUC of 0.845 (95% CI: 0.74–0.95), a sensitivity of 78.9% (95% CI: 0.63–0.90), a specificity of 86.7% (95% CI: 0.60–0.98), an accuracy of 81.1% (95% CI: 0.68–0.91), a positive predictive value (PPV) of 93.8% (95% CI: 0.79–0.99), and a negative predictive value (NPV) of 61.9% (95% CI: 0.38–0.82), demonstrating the best predictive performance. The combined model showed no statistically significant difference in AUC when compared with the independent predictors, including CTRW_α_10th percentile and CTRW_α_robust mean absolute deviation. However, the combined model also exhibited a higher AUC value compared to CTRW_α_10th percentile (0.845 *vs.* 0.691; P=0.091) and CTRW_α_robust absolute deviation (0.845 *vs.* 0.704; P=0.101). Moreover, in the comparison with CTRW_α_uniformity, the AUC of the combined model was significantly greater than the AUC obtained from CTRW_α_uniformity (0.845 *vs.* 0.688; P=0.005). The prediction performance of all models is shown in *Tables 3*,*4* and *Figure 3*.

Discussion

After binary logistic regression, this study ultimately identified six histogram features to construct a combined prediction model, including four CTRW_α features, DKI_K_minimum (the minimum value of diffusion kurtosis), and FROC_μ_10th percentile (the 10th percentile of the spatial parameter FROC_μ). Among them, CTRW_α_10th percentile, CTRW_α_robust mean absolute deviation, and CTRW_α_uniformity were independent predictive factors. The combined model showed the highest predictive performance of the Ki-67 PI compared with each single predictive factor (AUC =0.845, accuracy =78.9%, sensitivity =86.7%, and specificity =81.1%). Specifically, all the three of independent predictive factors were α-related features derived from the CTRW model, which indicated that the CTRW model was superior to other models and that the α parameter was the most useful parameter from the CTRW model. Overall, our study provides a novel noninvasive approach for the preoperative evaluation of the

Table 3 Univariable and multivariable logistic regression analysis of various diffusion indicators for distinguishing Ki-67 PI ≤50% and Ki-67 PI >50%

Parameter	Multivariable logistic regression		
	β value	OR (95% CI)	P value
CTRW_α_10th percentile	−0.046	0.955 (0.92–0.99)	0.019*
CTRW_α_mean	0.045	1.046 (1.00–1.10)	0.069
CTRW_α_robust mean absolute deviation	−0.113	0.893 (0.81–0.99)	0.028*
CTRW_α_uniformity	−9.448	0.000 (0.00–0.90)	0.047*
DKI_K_minimum	−0.006	0.994 (0.99–1.00)	0.088
FROC_μ_10th percentile	−0.001	0.999 (0.996–1.00)	0.262

*, P<0.05 indicates statistical significance. PI, proliferation index; OR, odds ratio; CI, confidence interval; CTRW_α, α value of continuous-time random walk; DKI_K, mean kurtosis value of diffusion kurtosis imaging; FROC_μ, μ value of fractional order calculus.

Table 4 Diagnostic performance of diffusion MRI quantitative metrics in discriminating Ki-67 PI ≤50% and Ki-67 PI >50%

Parameter	AUC (95% CI)	Sensitivity (%) (95% CI)	Specificity (%) (95% CI)	Accuracy (%) (95% CI)	PPV (%) (95% CI)	NPV (%) (95% CI)
CTRW_α_10th percentile	0.691 (0.54–0.84)	84.2 (0.68–0.94)	60.0 (0.32–0.84)	77.4 (0.64–0.88)	84.2 (0.69–0.94)	60.0 (0.32–0.84)
CTRW_α_robust mean absolute deviation	0.704 (0.56–0.85)	13.2 (0.04–0.28)	46.7 (0.21–0.73)	22.6 (0.12–0.36)	38.5 (0.14–0.68)	17.5 (0.07–0.33)
CTRW_α_uniformity	0.688 (0.54–0.84)	94.7 (0.82–0.99)	46.7 (0.21–0.73)	81.1 (0.68–0.91)	81.8 (0.67–0.92)	77.8 (0.40–0.97)
Combined model	0.845 (0.74–0.95)	78.9 (0.63–0.90)	86.7 (0.60–0.98)	81.1 (0.68–0.91)	93.8 (0.79–0.99)	61.9 (0.38–0.82)

Combined model: CTRW_α_10th percentile + CTRW_α_ mean + CTRW_α_robust mean absolute deviation + CTRW_α_ uniformity + DKI_K_ minimum+ FROC_μ_10th percentile. MRI, magnetic resonance imaging; PI, proliferation index; AUC, area under the curve; CI, confidence interval; PPV, positive predictive value; NPV, negative predictive value; CTRW_α, α value of continuous-time random walk; DKI_K, mean kurtosis value of diffusion kurtosis imaging; FROC_μ, μ value of fractional order calculus.

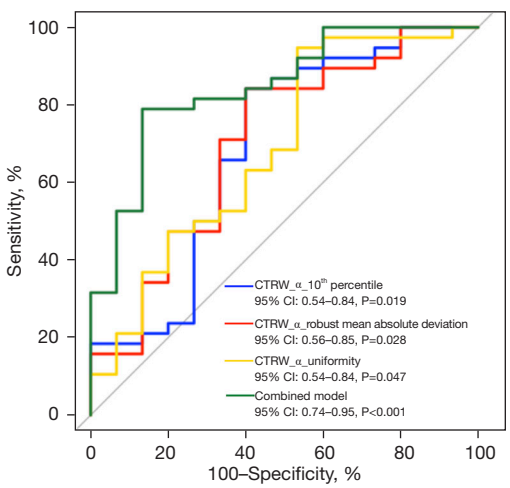

Figure 3 The receiver operating characteristic curves of the single mean apparent propagator CTRW_α_10th percentile, CTRW_α_robust mean absolute deviation, CTRW_α_uniformity, and the combined model. CTRW_α, α value of continuous-time random walk; CI, confidence interval.

Ki-67 PI.

Ki-67 is a marker for evaluating the proliferative activity status of tumors. Preoperative evaluation of the Ki-67 PI is central to treatment planning, prediction of treatment response, and the prognosis of patients with CC (19). In this paper, we propose, for the first time, the histogram features of multiple parameters obtained from four advanced non-Gaussian models, including IVIM, DKI, CTRW, and FROC, in evaluating the Ki-67 PI of CC. The AUC of our combined prediction model was 0.845, which was higher than that reported previously (AUC =0.816) (10). In this previous study, the texture features of IVIM parameters were demonstrated to be able to estimate the Ki-67 PI in CC. The ADC values obtained from DWI sequences are typically affected by vascular perfusion. IVIM can be used to effectively expose the diffusion information and blood microcirculation perfusion in tumor tissues through application of a double exponential model to distinguish

the diffusion movement of water molecules and blood flow microperfusion (20). The increased tumor PI commonly implies an increase in tumor density and the enrichment of angiogenesis within the tumor, which will increase the heterogeneity of the tumor. Although IVIM avoids blood perfusion influencing ADC values, thus providing more accurate D values, it cannot intuitively capture tissue heterogeneity. In contrast, our combined prediction model mainly incorporated the histogram features of parameter α obtained from CTRW but failed to include the relevant features of IVIM. Our results demonstrated a better predictive performance from only the texture features of IVIM than that reported previously, indicating that our prediction model obtained from four non-Gaussian distribution diffusion models had a better correlation with the Ki-67 PI and had certain advantages in capturing tumor heterogeneity in CC.

In our study, we ultimately selected three α-relevant histogram features out of the 162 histogram features as independent predictive factors, which were CTRW_α_10^{th} percentile, CTRW_α_robust mean absolute deviation, and CTRW_α_uniformity. All of these independent predictive factors were all derived from the CTRW diffusion model. The CTRW diffusion model can use a greater number of b values, including higher b values, rendering it more sensitive to tumor tissue structure (21). In our study, tumors in the group with high Ki-67 PI had higher values in α-related metrics from the CTRW diffusion model compared to the group with low Ki-67 PI, and only α-relevant features but no β-relevant features in this model were included as independent predictive factors. In the CTRW diffusion model, α and β are two quantitative parameters that can reflect the heterogeneity within the tissue structure voxel. Parameter α is related to the heterogeneity of diffusion time, describing the varying times required for water molecules to move within complex tissues and environments (22,23), and parameter β describes the diffusion of water molecules under asynchronous length (24). The increased Ki-67 PI in malignant tumors suggests an increased number and density of tumor cells and a greater unevenness in the microstructures (25). These heterogenous features ultimately resulted in the elevated value of parameters α and β in our study. In addition, the increase of Ki-67 implies an increase in tumor density and heterogeneity, which leads to a longer movement time for water molecules, resulting in higher α but not β value. This result indicates that α values are more strongly correlated with Ki-67 expression, which is consistent with previous studies on breast cancer and the Ki-67 PI (12).

We further found that the mean value of α was not significantly different between the high and low Ki-67 PI groups. Only the CTRW_α_10^{th} percentile, CTRW_α_robust mean absolute deviation, and CTRW_α_uniformity were included as the independent predictive factors. The 10^{th} percentile represents the tenth percentile of the α value. The average distance between each intensity value and the picture array's mean value is known as the mean absolute deviation. An increased uniformity suggests a stronger homogeneity or a smaller range of discrete intensity values. Uniformity is a measure of the sum of the squares of each intensity value and may indicate the homogeneity of the picture array (22). In our study, this result implied that the average values of α cannot always comprehensively reflect the heterogeneity of tumor tissues. Instead, histogram features may provide more information related to tumor heterogeneity. Moreover, the uniformity of the α parameter had the highest sensitivity for predicting the Ki-67 PI, which may be due a higher Ki-67 PI being correlated with a greater heterogeneity of the tumor. Although uniformity has certain advantages in reflecting the heterogeneity within tumors, its specificity is relatively low. Nevertheless, the comprehensive model that combined these three independent predictive factors yielded the highest AUC and good sensitivity, specificity, NPV, and PPV.

In this study, besides the strong correlation between the histogram features of CTRW and Ki-67 PI, among the four non-Gaussian diffusion models, the derived parameters of DKI_D and DKI_K in the DKI model were correlated with the Ki-67 PI, particularly the histogram feature K_minimum of DKI_K. This feature was included in the final combination prediction model through logistic regression. In the assessment of tumor proliferation, the DKI_D value of the DKI diffusion model was more similar to the conventional ADC value, resulting in a slightly weaker correlation with Ki-67 compared to DKI_K. This finding aligns with a previous study, which compared the parameters of IVIM and DKI for evaluating Ki-67 expression in soft tissue sarcoma and concluded that the DKI_K value of DKI is the optimal parameter for evaluating Ki-67 expression among the two models (26). Additionally, we also identified a correlation between Ki-67 PI and the μ value derived from FROC diffusion model. The unique parameter of μ represents the average free length of water molecules. The μ value increases when tumor cell proliferation activity grows, cell density increases, and the free diffusion of water molecules

diminishes. This finding is in line with earlier studies on lung cancer (27). Our investigation revealed no discernible relationship between Ki-67 PI and the histogram features of the IVIM diffusion model for either D* or f values. This could be because some cases of CC with high Ki-67 PI do not exhibit high perfusion due to the tumorous hypoxia, and the D* value is significantly affected by signal-to-noise ratio. This finding is in line with some studies on soft tissue sarcomas (26), lung cancer (28), nasal bone malignancies (29), and malignant ovarian epithelial tumors (30). Additionally, some research suggests that D* and f exhibits weak repeatability and reproducibility, thus producing a variability in results (31,32).

Our study had certain limitations which should be acknowledged. First, the study population size was relatively small, and patients were from a single center. Subsequent studies with larger and multicenter samples should be conducted to confirm our findings. Second, the choice of the best b value of the CTRW diffusion model in patients with CC remains to be investigated, and the established prediction model did not include the ADC value of the conventional diffusion sequence. A comparison of the prediction performance between the CTRW model and conventional DWI is needed. Third, in the DKI model, we could not determine whether the image noise with high b values was Rician noise or Gaussian noise although this does not affect our results. Finally, the surgical specimen for the pathological examination of Ki-67 was not a slice-to-slice correspondence with the MR images.

Conclusions

The whole-tumor histogram features derived from the multiple diffusion models can effectively predict the Ki-67 PI in patients with CC. The application of this predictive tool could potentially provide significant benefits in guiding preoperative treatment decisions and ultimately improving the prognosis for individuals with CC.

Acknowledgments

Funding: None.

Footnote

Reporting Checklist: The authors have completed the STROBE reporting checklist. Available at https://qims.amegroups.com/article/view/10.21037/qims-24-576/rc

Conflicts of Interest: All authors have completed the ICMJE uniform disclosure form (available at https://qims.amegroups.com/article/view/10.21037/qims-24-576/coif). The authors have no conflicts of interest to declare.

Ethical Statement: The authors are accountable for all aspects of the work in ensuring that questions related to the accuracy or integrity of any part of the work are appropriately investigated and resolved. This study was conducted in accordance with the Declaration of Helsinki (as revised in 2013) and was approved by the Institutional Ethics Committee of Sun Yat-sen Memorial Hospital of Sun Yat-sen University (No. SYSEC-KY-KS-2022-057). Informed consent was obtained from all individual participants.

References

1. Sung H, Ferlay J, Siegel RL, Laversanne M, Soerjomataram I, Jemal A, Bray F. Global Cancer Statistics 2020: GLOBOCAN Estimates of Incidence and Mortality Worldwide for 36 Cancers in 185 Countries. CA Cancer J Clin 2021;71:209-49.
2. Kyroudis CA, Dionysiou DD, Kolokotroni EA, Stamatakos GS. Studying the regression profiles of cervical tumours during radiotherapy treatment using a patient-specific multiscale model. Sci Rep 2019;9:1081.
3. Yamada I, Oshima N, Miyasaka N, Wakana K, Wakabayashi A, Sakamoto J, Saida Y, Tateishi U, Kobayashi D. Texture Analysis of Apparent Diffusion Coefficient Maps in Cervical Carcinoma: Correlation with Histopathologic Findings and Prognosis. Radiol Imaging Cancer 2020;2:e190085.
4. R DP, Arunachalam S, Amitkumar K, John JJ, Sudalaimuthu M. An Immunohistochemical Study on Ki-67 Expression in Squamous Cell Carcinomas of Cervix With Clinicopathological Correlation. Cureus 2023;15:e34155.

5. Song SE, Cho KR, Cho Y, Kim K, Jung SP, Seo BK, Woo OH. Machine learning with multiparametric breast MRI for prediction of Ki-67 and histologic grade in early-stage luminal breast cancer. Eur Radiol 2022;32:853-63.
6. Feng P, Shao Z, Dong B, Fang T, Huang Z, Li Z, Fu F, Wu Y, Wei W, Yuan J, Yang Y, Wang Z, Wang M. Application of diffusion kurtosis imaging and (18)F-FDG PET in evaluating the subtype, stage and proliferation status of non-small cell lung cancer. Front Oncol 2022;12:989131.
7. Zheng YM, Chen J, Zhang M, Wu ZJ, Tang GZ, Zhang Y, Dong C. CT radiomics nomogram for prediction of the Ki-67 index in head and neck squamous cell carcinoma. Eur Radiol 2023;33:2160-70.
8. Zhang G, Yan R, Liu W, Jin X, Wang X, Wang H, Li Z, Shang J, Wang K, Guo J, Han D. Use of biexponential and stretched exponential models of intravoxel incoherent motion and dynamic contrast-enhanced magnetic resonance imaging to assess the proliferation of endometrial carcinoma. Quant Imaging Med Surg 2023;13:2568-81.
9. Zhang Y, Zhou Y, Mao F, Yao R, Sun Q. Ki-67 index, progesterone receptor expression, histologic grade and tumor size in predicting breast cancer recurrence risk: A consecutive cohort study. Cancer Commun (Lond) 2020;40:181-93.
10. Li C, Zheng M, Zheng X, Fang X, Dong J, Wang C, Wang T. Predictive Ki-67 Proliferation Index of Cervical Squamous Cell Carcinoma Based on IVIM-DWI Combined with Texture Features. Contrast Media Mol Imaging 2021;2021:8873065.
11. Balyasnikova S, Brown G. Optimal Imaging Strategies for Rectal Cancer Staging and Ongoing Management. Curr Treat Options Oncol 2016;17:32.
12. Qin Y, Tang C, Hu Q, Yi J, Yin T, Ai T. Assessment of Prognostic Factors and Molecular Subtypes of Breast Cancer With a Continuous-Time Random-Walk MR Diffusion Model: Using Whole Tumor Histogram Analysis. J Magn Reson Imaging 2023;58:93-105.
13. Li HM, Zhang R, Gu WY, Zhao SH, Lu N, Zhang GF, Peng WJ, Qiang JW. Whole solid tumour volume histogram analysis of the apparent diffusion coefficient for differentiating high-grade from low-grade serous ovarian carcinoma: correlation with Ki-67 proliferation status. Clin Radiol 2019;74:918-25.
14. Huang C, Zhan C, Hu Y, Yin T, Grimm R, Ai T. Histogram analysis of breast diffusion kurtosis imaging: a comparison between readout-segmented and single-shot echo-planar imaging sequence. Quant Imaging Med Surg 2023;13:735-46.
15. Le Bihan D, Breton E, Lallemand D, Aubin ML, Vignaud J, Laval-Jeantet M. Separation of diffusion and perfusion in intravoxel incoherent motion MR imaging. Radiology 1988;168:497-505.
16. Jensen JH, Helpern JA, Ramani A, Lu H, Kaczynski K. Diffusional kurtosis imaging: the quantification of non-gaussian water diffusion by means of magnetic resonance imaging. Magn Reson Med 2005;53:1432-40.
17. Zhong Z, Merkitch D, Karaman MM, Zhang J, Sui Y, Goldman JG, Zhou XJ. High-Spatial-Resolution Diffusion MRI in Parkinson Disease: Lateral Asymmetry of the Substantia Nigra. Radiology 2019;291:149-57.
18. Sui Y, Wang H, Liu G, Damen FW, Wanamaker C, Li Y, Zhou XJ. Differentiation of Low- and High-Grade Pediatric Brain Tumors with High b-Value Diffusion-weighted MR Imaging and a Fractional Order Calculus Model. Radiology 2015;277:489-96.
19. Tu Y, Jiang P, Zhang J, Jiang S, Yi Q, Yuan R. The positive threshold of the immunohistochemical parameter Ki67 for predicting the recurrence of cervical cancer. Int J Gynaecol Obstet 2022;158:330-7.
20. Zhang Y, Zhang K, Jia H, Xia B, Zang C, Liu Y, Qian L, Dong J. IVIM-DWI and MRI-based radiomics in cervical cancer: Prediction of concurrent chemoradiotherapy sensitivity in combination with clinical prognostic factors. Magn Reson Imaging 2022;91:37-44.
21. Li C, Wen Y, Xie J, Chen Q, Dang Y, Zhang H, Guo H, Long L. Preoperative prediction of VETC in hepatocellular carcinoma using non-Gaussian diffusion-weighted imaging at high b values: a pilot study. Front Oncol 2023;13:1167209.
22. Su GH, Xiao Y, You C, Zheng RC, Zhao S, Sun SY, Zhou JY, Lin LY, Wang H, Shao ZM, Gu YJ, Jiang YZ. Radiogenomic-based multiomic analysis reveals imaging intratumor heterogeneity phenotypes and therapeutic targets. Sci Adv 2023;9:eadf0837.
23. Karaman MM, Sui Y, Wang H, Magin RL, Li Y, Zhou XJ. Differentiating low- and high-grade pediatric brain tumors using a continuous-time random-walk diffusion model at high b-values. Magn Reson Med 2016;76:1149-57.
24. Mehta R, Bu Y, Zhong Z, Dan G, Zhong PS, Zhou C, Hu W, Zhou XJ, Xu M, Wang S, Karaman MM. Characterization of breast lesions using multi-parametric diffusion MRI and machine learning. Phys Med Biol 2023. doi: 10.1088/1361-6560/acbde0.
25. Feng H, Liu H, Wang Q, Song M, Yang T, Zheng L, Wu

D, Shao X, Shi G. Breast cancer diagnosis and prognosis using a high b-value non-Gaussian continuous-time random-walk model. Clin Radiol 2023;78:e660-7.
26. Zhang K, Dai Y, Liu Y, Tao J, Pan Z, Xie L, Wang S. Soft tissue sarcoma: IVIM and DKI parameters correlate with Ki-67 labeling index on direct comparison of MRI and histopathological slices. Eur Radiol 2022;32:5659-68.
27. Luo Y, Jiang H, Meng N, Huang Z, Li Z, Feng P, Fang T, Fu F, Yuan J, Wang Z, Yang Y, Wang M. A comparison study of monoexponential and fractional order calculus diffusion models and (18)F-FDG PET in differentiating benign and malignant solitary pulmonary lesions and their pathological types. Front Oncol 2022;12:907860.
28. Zheng Y, Huang W, Zhang X, Lu C, Fu C, Li S, Lin G. A Noninvasive Assessment of Tumor Proliferation in Lung cancer Patients using Intravoxel Incoherent Motion Magnetic Resonance Imaging. J Cancer 2021;12:190-7.
29. Xiao Z, Zhong Y, Tang Z, Qiang J, Qian W, Wang R, Wang J, Wu L, Tang W, Zhang Z. Standard diffusion-weighted, diffusion kurtosis and intravoxel incoherent motion MR imaging of sinonasal malignancies: correlations with Ki-67 proliferation status. Eur Radiol 2018;28:2923-33.
30. Song XL, Wang L, Ren H, Wei R, Ren JL, Niu J. Intravoxel Incoherent Motion Imaging in Differentiation Borderline From Malignant Ovarian Epithelial Tumors: Correlation With Histological Cell Proliferation and Vessel Characteristics. J Magn Reson Imaging 2020;51:928-35.
31. Dyvorne HA, Galea N, Nevers T, Fiel MI, Carpenter D, Wong E, Orton M, de Oliveira A, Feiweier T, Vachon ML, Babb JS, Taouli B. Diffusion-weighted imaging of the liver with multiple b values: effect of diffusion gradient polarity and breathing acquisition on image quality and intravoxel incoherent motion parameters--a pilot study. Radiology 2013;266:920-9.
32. Liu C, Wang K, Chan Q, Liu Z, Zhang J, He H, Zhang S, Liang C. Intravoxel incoherent motion MR imaging for breast lesions: comparison and correlation with pharmacokinetic evaluation from dynamic contrast-enhanced MR imaging. Eur Radiol 2016;26:3888-98.

Cite this article as: Su Y, Zeng K, Yan Z, Yang X, Yang L, Yang L, Han R, Huang F, Deng H, Duan X. Predicting the Ki-67 proliferation index in cervical cancer: a preliminary comparative study of four non-Gaussian diffusion-weighted imaging models combined with histogram analysis. Quant Imaging Med Surg 2024;14(10):7484-7495. doi: 10.21037/qims-24-576

